Rock Mechanics Bulletin 2 (2023) 100042

Contents lists available at ScienceDirect

Rock Mechanics Bulletin

journal homepage: www.keaipublishing.com/en/journals/rock-mechanics-bulletin

Hyper-gravity experiment of solute transport in fractured rock and evaluation method for long-term barrier performance

Wenjie Xu [a,b], Yingtao Hu [c,d,e,*], Yunmin Chen [a,b], Liangtong Zhan [a,b], Ruiqi Chen [a,b], Jinlong Li [a,b], Duanyang Zhuang [a,b], Qingdong Li [a,b], Ke Li [a,b]

[a] Center for Hyper-gravity Experimental and Interdisciplinary Research, Zhejiang University, Hangzhou, 310058, China
[b] MOE Key Laboratory of Soft Soils and Geoenvironmental Engineering, Zhejiang University, Hangzhou, 310058, China
[c] Department of Civil Engineering, Hangzhou City University, Hangzhou, 310015, China
[d] Key Laboratory of Safe Construction and Intelligent Maintenance for Urban Shield Tunnels of Zhejiang Province, Hangzhou, 310015, China
[e] Advanced Materials Additive Manufacturing Innovation Research Center, Hangzhou City University, 310015, China

ARTICLE INFO

Keywords:
Hyper-gravity effect
Fractured rock
3D printed fracture
Solute transport
Long-term

ABSTRACT

Hyper-gravity experiment enable the acceleration of the long-term transport of contaminants through fractured geological barriers. However, the hyper-gravity effect of the solute transport in fractures are not well understood. In this study, the sealed control apparatus and the 3D printed fracture models were used to carry out 1 g and N g hyper-gravity experiments. The results show that the breakthrough curves for the 1 g and N g experiments were almost the same. The differences in the flow velocity and the fitted hydrodynamic dispersion coefficient were 0.97–3.12% and 9.09–20.4%, indicating that the internal fractures of the 3D printed fracture models remained stable under hyper-gravity, and the differences in the flow and solute transport characteristics were acceptable. A method for evaluating the long-term barrier performance of low-permeability fractured rocks was proposed based on the hyper-gravity experiment. The solute transport processes in the 1 g prototype, 1 g scaled model, and N g scaled model were simulated by the OpenGeoSys (OGS) software. The results show that the N g scaled model can reproduce the flow and solute transport processes in the 1 g prototype without considering the micro-scale heterogeneity if the Reynolds number (Re) ≤ critical Reynolds number (Re_{cr}) and the Peclet number (Pe) ≤ the critical Peclet number (Pe_{cr}). This insight is valuable for carrying out hyper-gravity experiments to evaluate the long-term barrier performance of low-permeability fractured porous rock.

1. Introduction

Deep geological disposal is an internationally recognized safe, reliable, and technically feasible method to prevent high-level radioactive waste leachate from escaping into the environment (Costin, 1997; Laverov et al., 1994; Mckinley et al., 2007; Wang et al., 2018). Granite is a typical low-permeability fractured porous medium and a key geological barrier. Since the design service life of an engineered barrier is about 1000 years, the long-term barrier performance of a deep disposal repository depends strongly on the granite barrier. However, the ability of the geological barrier to provide long-term service is directly related to the quality of the surrounding hydrogeological environment. Field monitoring of long-term transport processes is not possible. Therefore, hyper-gravity experiments enable the acceleration of the transport of contaminants through geological barriers.

In a 1/N-scale centrifuge model, the seepage path lengths are 1/N times shorter than in actual conditions. The self-weight of the pore fluid is N times larger in a centrifuge model with a centrifugal force of N g (i.e., at 500g, water weighs 500 times its weight at 1g). Thus, the local seepage velocity at any point is N times faster than in the prototype. Therefore, advective processes occur N^2 times faster in the model than in the prototype (Schofield, 1980; Taylor, 1995; Chen and Han et al., 2011; Ng, 2014). For example, a 14.6-day modeling period at 500 g can simulate advective transport processes that require more than ten thousand years in the prototype (14.6 days × 500^2 = 10,000 h). Thus, hyper-gravity experiments can accelerate transport processes in a small-scale model at stress levels similar to those experienced by the prototype.

The use of hyper-gravity experiments to simulate contaminant transport began in the late 1980s. Researchers studied the similitude of contaminant transport simulations, derived 8 dimensionless groups of

* Corresponding author. Department of Civil Engineering, Hangzhou City University, Hangzhou, 310015, China.
E-mail address: huyt@zucc.edu.cn (Y. Hu).

https://doi.org/10.1016/j.rockmb.2023.100042
Received 31 December 2022; Received in revised form 17 February 2023; Accepted 18 March 2023
Available online 23 March 2023

contaminant transport, explained the similarity conditions, and demonstrated the feasibility of simulating contaminant transport by hyper-gravity experiments (Arulanandan et al., 1988; Griffioen and Barry, 1999; Hensley and Schofield, 1991; Kumar and Singh, 2012; Lo et al., 2004; Soga et al., 2003; Zhan et al., 2022a,b). For instance, Hensley and Schofield (1991) conducted hyper-gravity experiments on the long-term transport of NaCl in silt. The test lasted 27 h under 100 g centrifugal acceleration, simulating 31 years of solute transport process in a landfill. Lo et al. (2005) simulated the one-dimensional transport of adsorptive inorganic contaminants (such as cadmium) in saturated and unsaturated soils. Zhang and Hu (2006) studied the long-term transport behavior of light non-aqueous phase liquids (LNAPLs) in unsaturated soil. The test results showed that the hyper-gravity experiments accurately simulated the transport processes of LNAPLs in unsaturated soil. Zeng (2015) carried out a 72-h hyper-gravity experiment under 50 g centrifugal acceleration to simulate Pb^{2+} transport through a kaolin liner using a ZJU-400 centrifuge developed by Zhejiang University. The continuous test reproduced 22.8 years of solute breakthrough processes in a 2-m thick compacted clay layer, verifying the long-term barrier performance of the clay barrier. Subsequently, Zhan et al. (2022) conducted a test at an acceleration of 100 g for 43.8 h to simulate 50 years of contaminant transport in soil-bentonite walls and loess-amended soil-bentonite walls. Their results verified the 50-year long-term barrier performance of the loess-modified barrier. These studies demonstrate that hyper-gravity experiments are effective for predicting the long-term barrier performance of fractured rock masses with low permeability.

However, due to the discontinuity and heterogeneity of fractured rock masses, it is difficult to use prototype materials to create a model, and there is no similar suitable material to prepare a similar model. Only a few studies have reported hyper-gravity experiments of flow and solute transport in fractured media (Brouwers and Dippenaar, 2018; Gurumoorthy and Singh, 2004; Jones et al., 2017, 2018; Levy et al., 2002, 2003; Nishimoto et al., 2016; Sawada et al., 2017). Levy et al. (2002, 2003) investigated the potential of a geotechnical centrifuge as an experimental tool to study the infiltration of dense non-aqueous phase liquids (DNAPL) into a fracture system. They analyzed microscopic fractures (Culligan and Barry, 1998) and observed a very good agreement between the scaled test and the prototype data if the effects of the inertial forces were negligible. Subsequently, Jones et al. (2017) carried out hyper-gravity experiments on the flow of potassium permanganate crystals in a single plexiglass fracture model under different flow rates at 20 g. The results proved that the hyper-gravity experiments could be used to simulate and observe the fracture flow processes. Jones et al. (2018) conducted Lugeon tests using geotechnical centrifuge modeling to investigate the flow behavior through an inclined smooth single-fracture model. The research results showed that the width of the dominant flow path increased with an increase in the inflow pressure. However, the measured flow velocity was large, with *Re* ranging from 169 to 698, and there was a nonlinear relationship between the pressure and flux. Therefore, the similarity of the flow velocity remains to be analyzed. In addition, Gurumoorthy and Singh (2004) simulated the molecular diffusion of Cs^{+} and I^{-} in integrated granite or a single fracture using hyper-gravity experiments. However, they only considered molecular diffusion but ignored convection and mechanical dispersion. Nishimoto and Sawada (2016; 2017) conducted near-field hyper-gravity experiments to evaluate the geomechanical properties in the surrounding rock of a high-level radioactive waste geological disposal reservoir. Tests were conducted under a centrifugal force of 30 g in isotropic stress-constraint conditions with confining pressures of 5–10 MPa and an injection of pore water at the bottom of the model. The tests were conducted continuously for 67 days, reproducing the flow, mechanics, and temperature of the prototype during 165 years. The results demonstrated the feasibility of simulating the long-term characteristics of a geological disposal reservoir containing high-level radioactive waste and the long-term transport processes of solutes in fractured media using hyper-gravity experiments.

In summary, current hyper-gravity experiments of solutes or contaminant transport have only been conducted in soil media. There are few reports on experimental studies on the flow and solute transport in fractured rock masses, and the hyper-gravity effect and similarity of the solute transport in fractures are not well understood. Therefore, it is necessary to study the hyper-gravity effect of solute transport in a fractured rock mass to develop experimental methods and provide theoretical support for subsequent hyper-gravity experiments of solute transport in low-permeability fractured rock masses.

This study investigates solute transport in a fractured rock mass using hyper-gravity experiments and develops an evaluation method for long-term barrier performance. 3D-printed fracture models and a custom-made sealed control apparatus were used to carry out normal gravity and hyper-gravity experiments of solute transport in a fractured rock mass. The feasibility of the 3D printed fracture model for hyper-gravity experiments of solute transport in a fractured rock mass was evaluated, and the influence of hyper-gravity on the solute transport in a fractured rock mass was analyzed. A method for evaluating the long-term barrier performance of low-permeability fractured rocks is proposed based on the results of the hyper-gravity experiment. Solute transport processes in a 1 g prototype,1 g scaled model, and N g scaled model are simulated. The results provide some guidance for verifying the long-term barrier performance of deep-earth projects, such as the storage of high-level waste in geological disposal reservoirs.

2. Experimental method

2.1. Experimental setup

Solute transport tests of 3D-printed fractured rocks were performed using a hyper-gravity experimental apparatus to investigate the fluid flow and solute transport in a fractured rock mass. The device was developed by researchers at Zhejiang University (Fig. 1). The apparatus consists of a centrifuge (ZJU400), a sealed control unit containing the fractured rock, an upstream solute control unit, an upstream water level control unit, an effluent reservoir, a waste liquid collection reservoir, a valve control unit, and a data acquisition unit. The sealed control unit containing the fractured rock has 6 boundary interfaces and can simulate a maximum pore pressure of 5 MPa under a maximum centrifugal force of 100 g. It accommodates cube specimens with a maximum length of 200 mm. The device can simulate the in-situ stress of large-scale rock engineering in a reduced geo-mechanical model, specifically the vertical stress gradient induced by gravity. The hyper-gravity is the result of the high-speed rotation of the centrifuge. As shown in Fig. 1, the upstream water level was maintained by several Mariotte bottles (Thorel et al., 2002; Zhan et al., 2022a,b), which automatically provided a continuous supply of the solution supply during the rotation of the centrifuge. The downstream water level was controlled by a spillway of the downstream water level control unit. The hydraulic head was maintained by adjusting the height of the Mariotte bottles. The upstream water level was higher to create a flow, and the outflow solution was collected in the effluent reservoir.

2.2. Monitoring devices

As shown in Fig. 1, four micro-pore water pressure sensors (PPSs) (HC-25, ±0.1% accuracy) were attached to the inlet and outlet of the sealed control unit to monitor the inlet and outlet pressure of the fracture model, respectively. Two micro-pore water pressure sensors, one temperature sensor (Pt-100, ±0.1% accuracy), and one conductivity meter (EC-510, ±1.5% accuracy) were attached to the effluent reservoir. The three sensors were used to perform real-time monitoring of the water level, the temperature, and the cumulative conductivity of the outflow solution.

2.3. 3D printed fracture model

A method was developed to create 3D-printed models of a rock mass

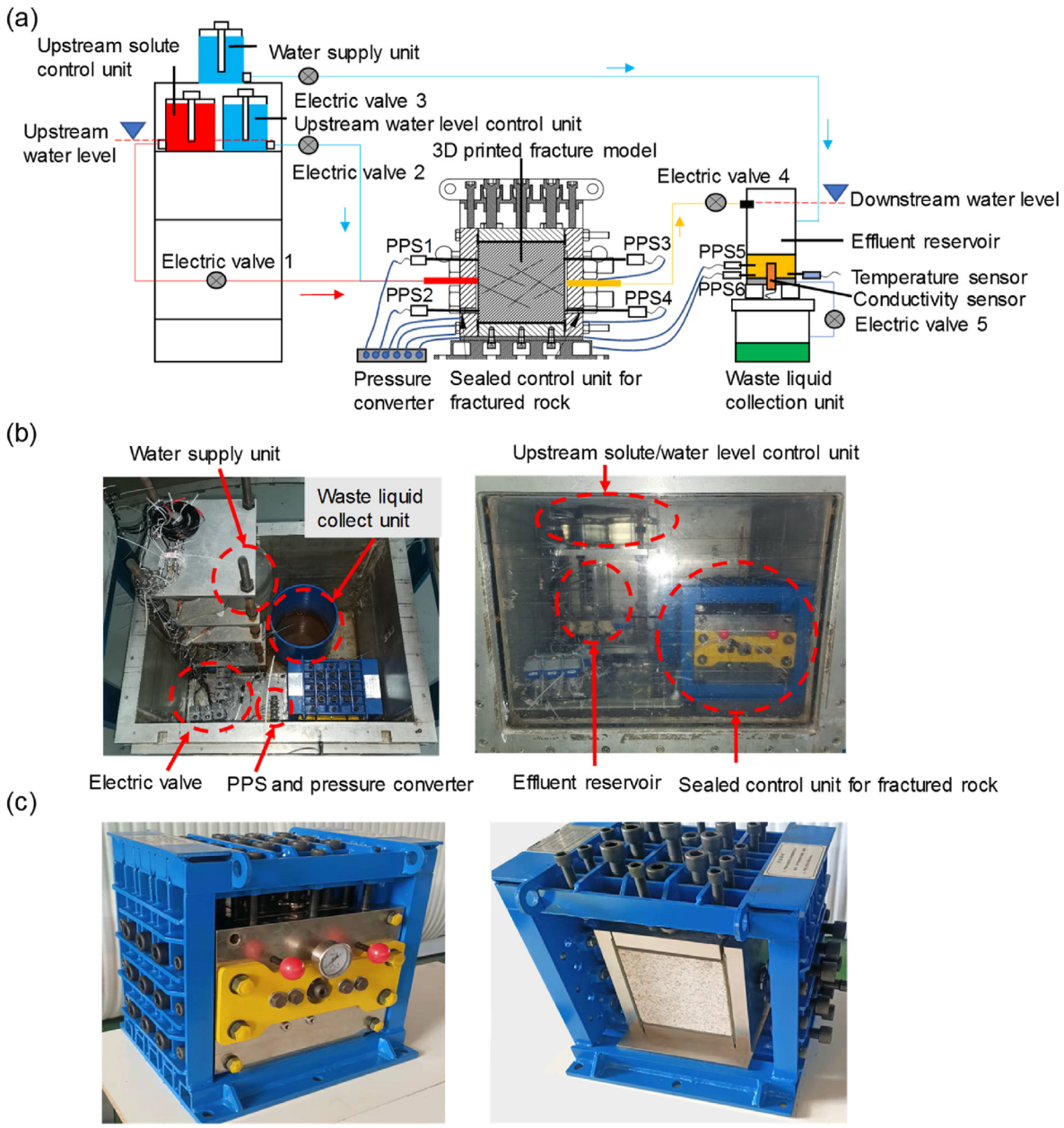

Fig. 1. The hyper-gravity experimental apparatus: (a) schematic diagram (the arrow represents the flow or solute transport direction); (b) layout in the model box; (c) the sealed control unit for fractured rock.

with a single fracture and a fracture network. Due to the high cost of 3D printing, only the key parts of the fracture model were printed, and other parts were replaced by aluminum alloy. Fig. 2a shows the variable-aperture single-fracture model (200 mm long × 200 mm width × 20 mm high). The initial fracture aperture was 0.5 mm due to the limitations of the 3D printing accuracy. The hardness of the printed rubber in the model was 65. This hardness level and the selected structure could produce realistic deformation of the fracture model under a given confining stress. In addition, it should be noted that the objective of this study is to clarify the effect of hyper-gravity on the flow and transport process in fractures, and the effect of rock matrix is not considered for simplify, which is printing with impermeable resin material.

Fig. 2b shows the 3D printed variable-aperture fracture network model (200 mm long × 100 mm wide × 100 mm high). The initial fracture aperture of each single fracture in the fracture network model are set the same (0.5 mm), and the rubber hardness (65) were the same as in the single-fracture model. The model consisted of the fracture network and the matrix. Several single fractures crossed the matrix and were connected by rubber, enabling the deformation by confining stress. The matrix supported the fracture network and had a hollow interior filled with sand and sealed with high-strength bolt plugs on the surface. This design substantially reduced the manufacturing cost and ensured the structural strength of the 3D printed model.

Fig. 3 shows the assembled 3D-printed fracture model and the layout scheme in the sealed control unit. The assembled fracture model experienced deformation under the confining stress exerted by the pressurization mechanism on both sides. Thus, the fracture aperture was limited to 0–0.5 mm. The implementation steps of the sealed control unit were as follows. First, the fracture of the assembled model was placed in the vertical direction, which is parallel to the direction of the centrifugal force under hyper-gravity. This setting ensured the formation of a gradient of the water pressure at the fracture boundary and prevented

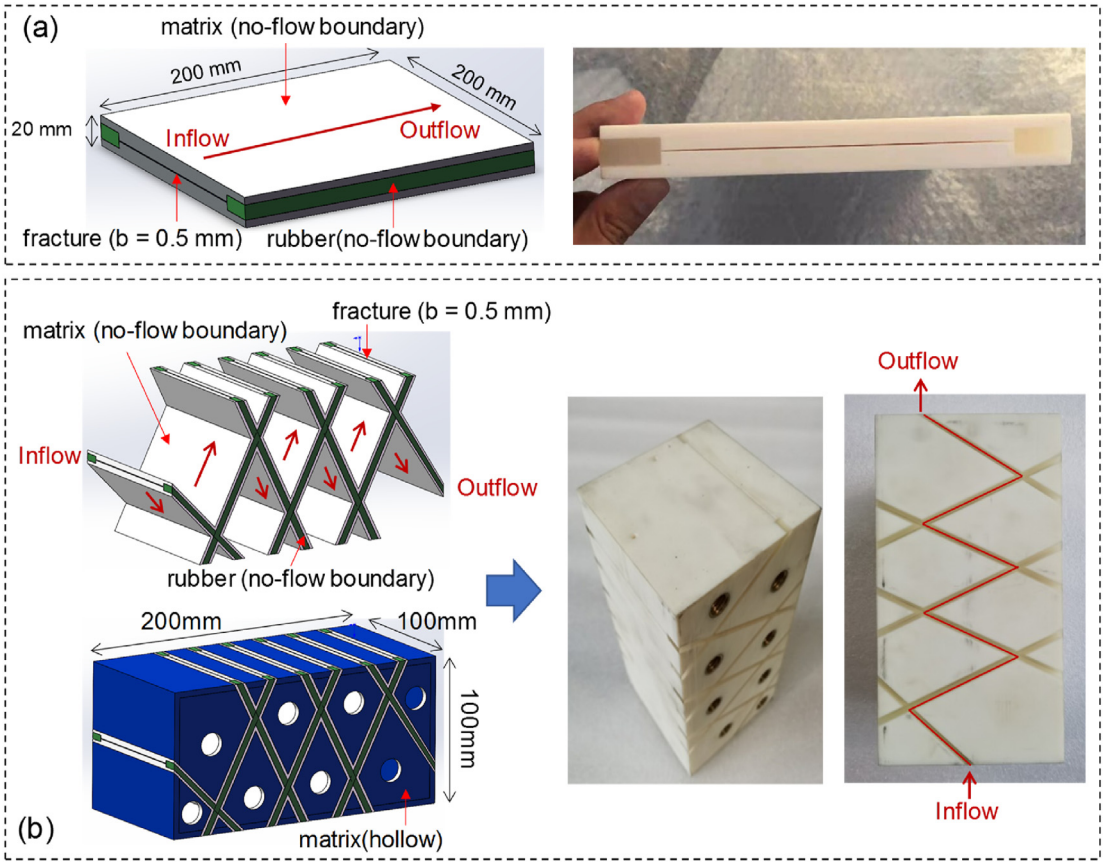

Fig. 2. 3D printed fracture model: (a) single-fracture model; (b) fracture network model.

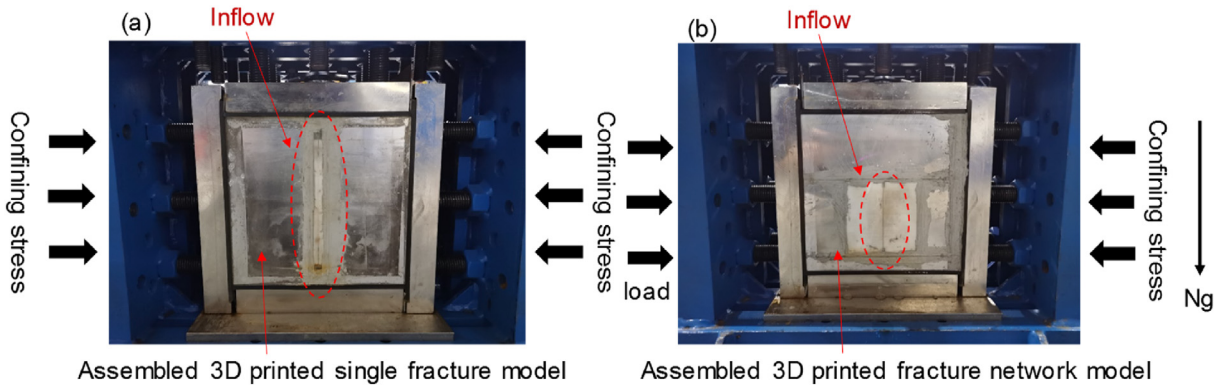

Fig. 3. 3D printed fracture model in the sealed control unit: (a) single-fracture model; (b) fracture network model.

secondary deformation under hyper-gravity. Second, after the six sides of the sealed control unit were assembled and sealed, a flow test was carried out to observe the flow changes. If the permeability was too high, we adjusted the confining stress to control the fracture aperture or the permeability.

2.4. Experimental plan

Normal gravity flow experiments were first carried out to design hyper-gravity experiments of the solute transport in the 3D printed fracture model. Fig. 4a shows the relationship between the pressure drop and the flow rate/Reynolds number (*Re*) during the flow experiments in the single-fracture model. The results indicated a linear relationship between the flow rate and the pressure drop, with the *Re* ranging from 0.25 to 1.061. Thus, Darcy's law is applicable. The average equivalent hydraulic fracture aperture was 2.18×10^{-5} m, and the permeability was 3.96×10^{-4} m/s.

According to the results of the flow experiments, three groups of solute transport experiments with different pressure differences and different g levels were designed under normal gravity and hyper-gravity (Table 1). The pressure differences of the normal gravity experiments were 100, 200, and 300 kPa, and the corresponding g levels of the hyper-gravity experiments were 20, 40, and 60 g to evaluate the influence of hyper-gravity on the solute transport in the 3D printed single-fracture model.

Fig. 4b shows the relationship between the pressure drop and flow rate/*Re* during the flow experiments in the fracture network model. The results also suggested a linear relationship, with the *Re* ranging from

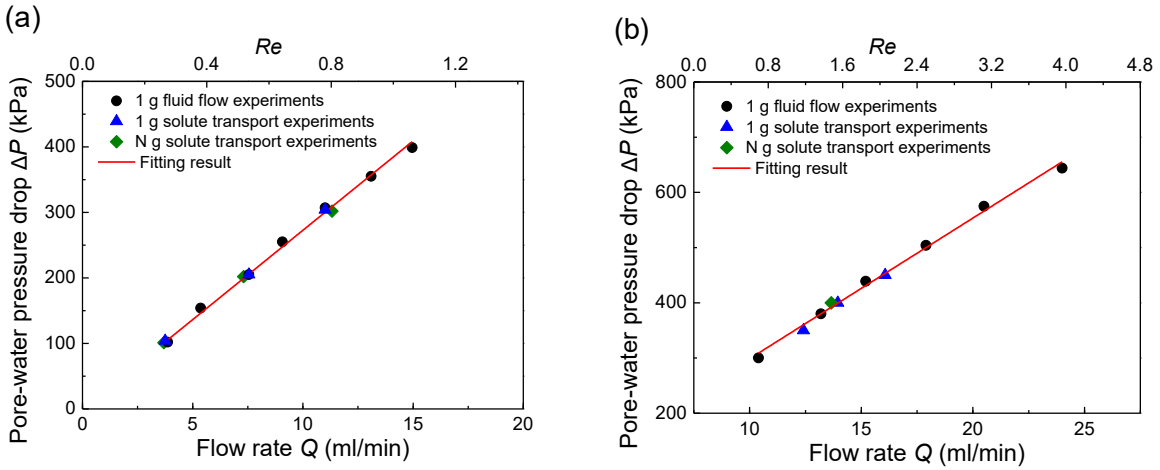

Fig. 4. Relationship between pressure drop and flow rate/Reynolds number during flow and transport experiments: (a) single-fracture model; (b) fracture network model.

Table 1
Experimental cases of solute transport in 3D printed single-fracture model.

Case	Number	G level	Head difference ΔH (cm)	Pressure difference ΔP (kPa)
normal gravity	S1	1 g	\	100
	S2		\	200
	S3		\	300
hyper-gravity	C1	20 g	50	100
	C2	40 g		200
	C3	60 g		300

1.659 to 3.828. Therefore, Darcy's law is valid in this experiment. The calculated average equivalent hydraulic fracture aperture was 2.85 × 10^{-5} m, and the permeability was 6.76 × 10^{-4} m/s. As shown in Table 2, three groups of normal gravity experiments and one hyper-gravity experiment at 80 g were designed. A comparison experiment with a pressure difference of 400 kPa under normal gravity and 80 g hyper-gravity was conducted to evaluate the influence of hyper-gravity on the solute transport in the 3D printed fracture network model.

3. Results and discussion

3.1. Test 1: Single-fracture model

3.1.1. The effect of hyper-gravity on the flow behavior

The pore water pressure difference between the inlet and outlet of the fracture model and the pore water pressure/water level in the effluent reservoir under normal gravity and hyper-gravity are shown in Fig. 5. The pressure differences were relatively stable in the normal gravity experiments (S1, S2, and S3) (Fig. 5a), with a range of ±2 kPa, indicating that the supply pressure was stable. As shown in Fig. 5c, the pore pressure/water level of S1, S2, and S3 increased over time, indicating that the solution flowed continuously into the effluent reservoir. The water level increased linearly, and the slope increased as the pressure difference increased.

Table 2
Experimental cases of solute transport in 3D printed fracture network model.

Case	Number	G level	Head difference ΔH (cm)	Pressure difference ΔP (kPa)
normal gravity	N1	1 g	\	350
	N2		\	400
	N3		\	450
hyper-gravity	D1	80 g	50	400

In the hyper-gravity experiments, the pressure difference ΔP was calculated by the average pressure between the inlet and outlet, P_{in} - P_{out}, and $P_{in} = (P_1+P_2)/2$, $P_{out} = (P_3+P_4)/2$. The results are shown in Fig. 5b. The effluent reservoir was equipped with PPSs 5 and 6 to monitor the real-time pressure P_5 and P_6. The results are shown in Fig. 5d–e. The slopes of the pore pressure and water level were similar, suggesting that the flow velocity in the 3D printed single-fracture model was relatively stable under hyper-gravity. The results of the hyper-gravity experiments also show that the slopes increased, indicating that the flow velocity in the fracture model increased with an increase in the g level.

The findings show that the flow characteristics of the solute transport in the 3D-printed single-fracture model were similar under 1 g and N g. The flow velocity and equivalent hydraulic fracture aperture under different experimental conditions are listed in Table 3. The difference in the equivalent hydraulic fracture aperture obtained from the normal gravity and hyper-gravity experiments was small, and the maximum difference in the flow velocity was 3.12%, demonstrating similar flow characteristics of the 3D printed single-fracture model under hyper-gravity and normal gravity. In addition, the flow velocity under different conditions increased N times with the pressure difference or centrifugal acceleration g level, and the *Re* was less than 1, indicating that the flow processes were similar under hyper-gravity and normal gravity.

The relationships between the flow pressure difference and flux of the normal gravity and hyper-gravity transport experiments were compared with those of the normal gravity flow experiments, as shown in Fig. 4a. The data obtained from the transport experiments were within the fitted curve derived from the flow experiments.

3.1.2. The effect of hyper-gravity on the transport behavior

Fig. 6 shows the cumulative conductivity/concentration curves and breakthrough curves (BTCs) derived from the normal gravity and hyper-gravity experiments for the single-fracture model. The conductivity sensor in the outlet effluent reservoir monitored the cumulative conductivity continuously. The duration time when the measured conductivity was measured in S1, S2, S3 and C1, C2, C3 shortened as the pressure increased (Fig. 6a), i.e., the breakthrough time of the solute transport in the fracture model was shortened. Unlike in the normal gravity experiments, the conductivity exhibited slight fluctuations under hyper-gravity because the environment affected the working performance of the conductivity sensor.

Based on the evolution of the concentration, the solute transport

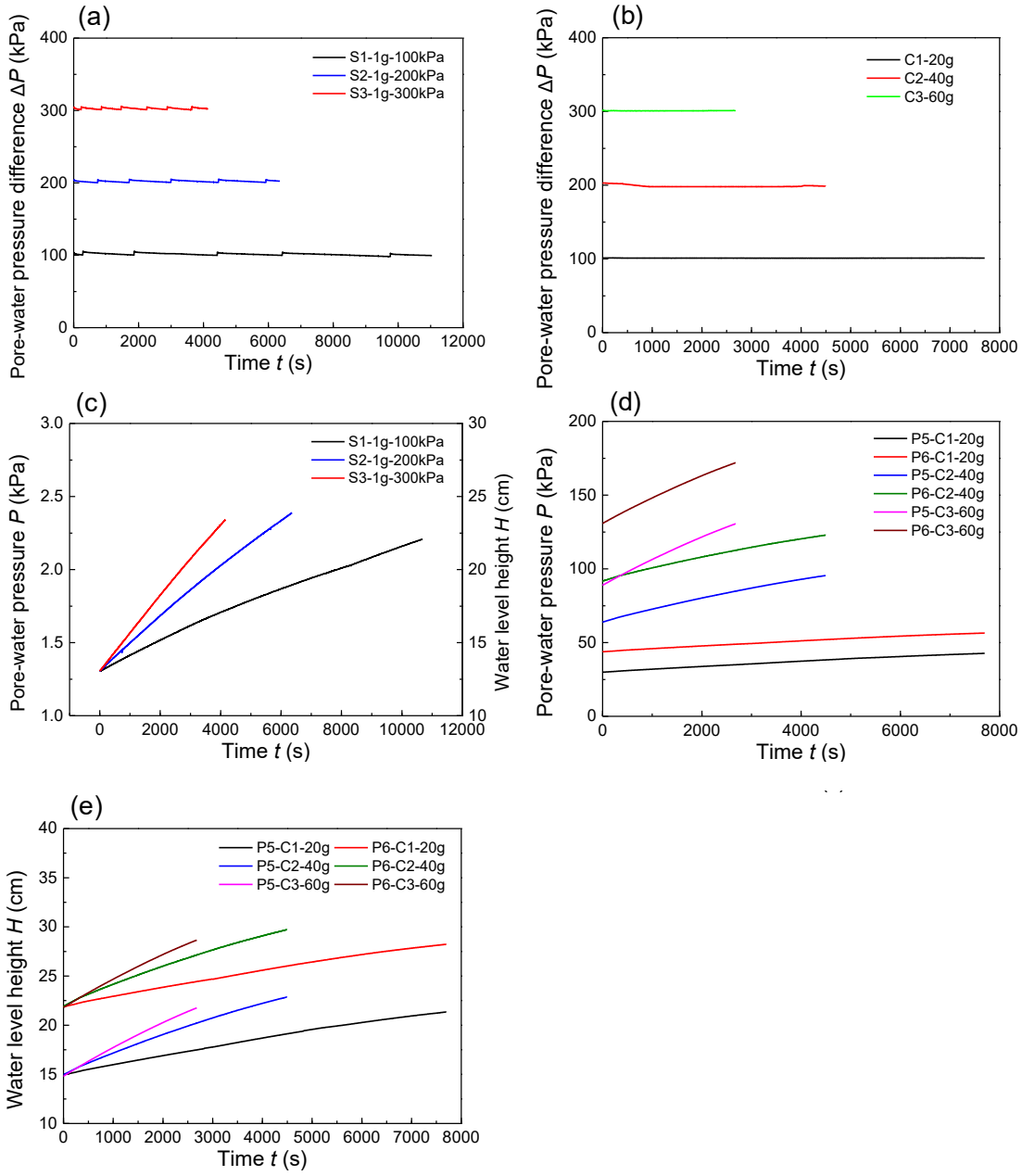

Fig. 5. Pore water pressure difference between the inlet and outlet under (a) normal gravity and (b) hyper-gravity; pore water pressure/water level in the effluent reservoir under (c) normal gravity and (d–e) hyper-gravity.

Table 3
Flow and solute transport characteristics in the 3D printed single-fracture model under 1 g and N g.

G level	Case	v (10^{-2} m/s)	b_h (10^{-5}m)	Re	Pe	$t_{0.1}$ (s) ($C/C_0 = 10\%$)	D_h (10^{-7} m^2/s)	ADE fitting error R^2
1 g	S1	1.587	2.187	0.266	171.021	1621	0.66	0.9936
	S2	3.175	2.203	0.536	344.548	859	1.10	0.9992
	S3	4.654	2.191	0.781	502.232	471	1.93	0.9974
20 g	C1	1.555	2.197	0.262	168.277	1549	0.53	0.9891
40 g	C2	3.091	2.190	0.518	333.522	952	1.20	0.9986
60 g	C3	4.731	2.216	0.803	516.454	490	1.75	0.9981

Notes: v, b_h, $t_{0.1}$, D_h represent the flow velocity, the hydraulic fracture aperture, the breakthrough time and the hydrodynamic dispersion coefficient, respectively.

process can be divided into the following three stages:

Stage I – solute infiltration: in the initial stage, the water level in the effluent reservoir rises, but the conductivity does not change because the solute flows into the inlet water chamber from the fracture inlet. At this time, the fracture model is flooded by the inflowing solution, which flows from the fracture outlet to the effluent reservoir. However, the solute has

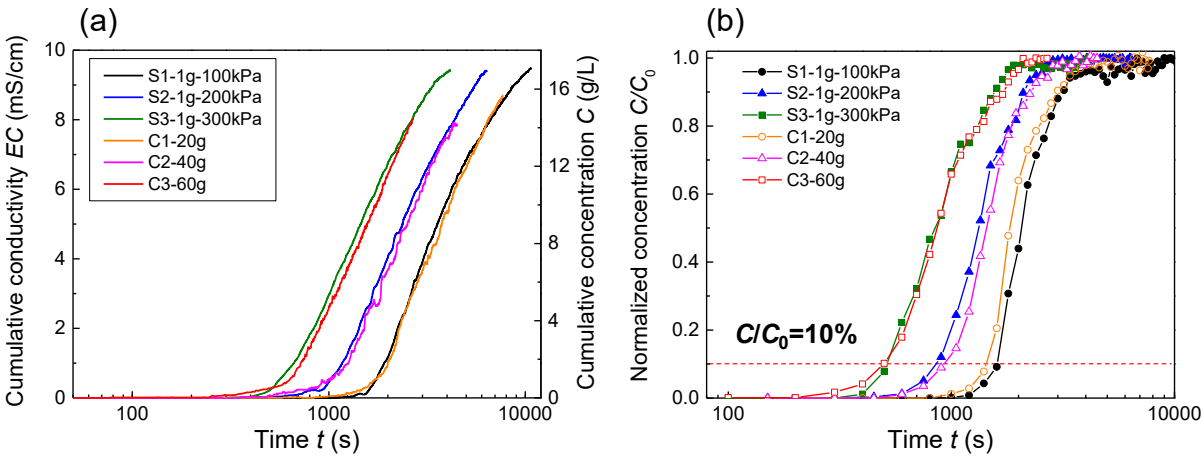

Fig. 6. Comparison of experimental results of normal gravity and hyper-gravity tests for the single-fracture model: (a) cumulative conductivity/concentration curves; (b) breakthrough curves (BTCs).

not yet reached the fracture outlet. Therefore, the conductivity in the effluent reservoir is the background value of pure water, and the cumulative solute mass is 0.

Stage II - solute breakthrough: in this stage, the conductivity curve exhibits a breakpoint, and the conductivity increases. At this time, the solute has infiltrated the fracture model, migrated to the fracture outlet, and flowed into the effluent reservoir. The outflow concentration and cumulative solute mass increased, resulting in an increase in the cumulative conductivity.

Stage III - solute saturation: the water in the inlet/outlet water chamber and fracture is gradually replaced by the solute, and the outflow concentration reaches the peak concentration or is close to the solution concentration. The rate of increase of the conductivity slows down significantly, but the cumulative solute mass is still increasing. It is worth noting that although the outflow concentration has reached the peak value, the cumulative conductivity is still rising. At this time, the outflow solution is diluted due to the water in the effluent reservoir, and the cumulative solution concentration in the effluent reservoir has not yet reached the maximum value.

Fig. 6 shows that the characteristics of the cumulative concentration curves are similar under 1 g and N g. The BTCs are slightly different, but the overall difference is small, indicating that the solute transport characteristics in the 3D-printed single-fracture model are the same under hyper-gravity and normal gravity.

We used the breakthrough standard in the Technical Code for Geotechnical Engineering of Domestic Waste Landfill (CJJ176-2012). The breakthrough time, $t_{0.1}$, of the solute transport in the fracture is defined based on the speed of the solute transport in the fracture model. Table 3 shows the calculated breakthrough time $t_{0.1}$ and Pe for different experimental cases, indicating that the breakthrough time of the solute decreases with an increase in the pressure or the g level.

The Advection-Diffusion (ADE) model was used to fit the normalized BTCs depicted in Fig. 6b to compare the solute transport characteristics under different conditions. The results are shown in Fig. 7. The hydrodynamic dispersion coefficient D_h and the coefficient of determination R^2 are listed in Table 3. The R^2 values are greater than 0.99, and D_h increases with an increase in the pressure or the g level. The relative difference in D_h between the normal gravity and hyper-gravity experiments ranges from 9.09% to 20.4%.

The temperature in the centrifuge chamber increases with an increase in the centrifugal acceleration (g level) and the operation time, changing the solution temperature in the experiments and affecting the dynamic viscosity coefficient of the fluid. Therefore, a temperature sensor was placed in the effluent reservoir to monitor the temperature of the outflow liquid to evaluate the possible influence of the liquid's temperature on the results. Fig. 8 shows the temperature of the fluid in the C1, C2, and C3 experiments. The temperature increases over time and with the g level. The maximum temperature difference between the different conditions is

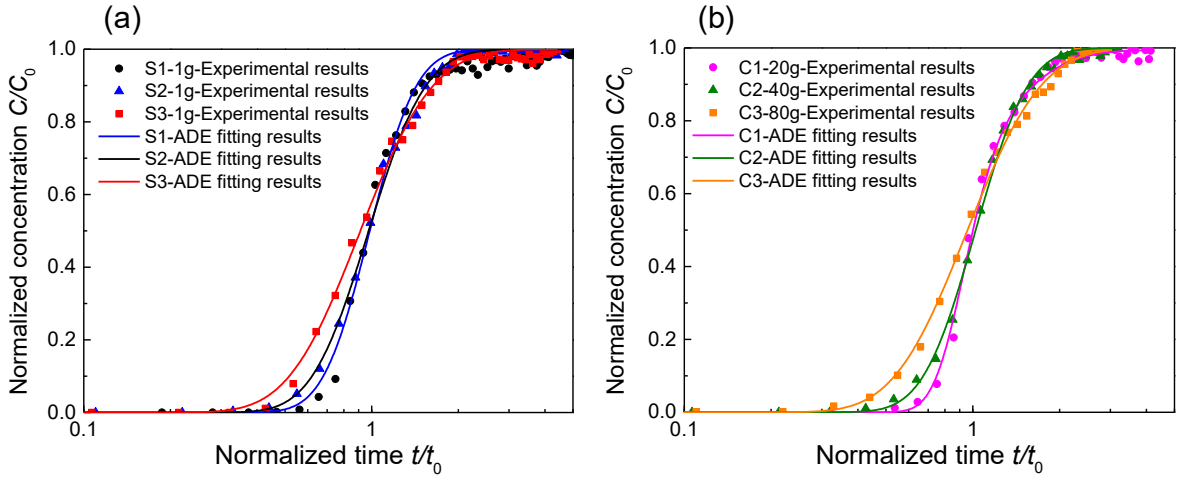

Fig. 7. Fitting curves of normalized outflow concentration for the single-fracture model: (a) normal gravity; (b) hyper-gravity.

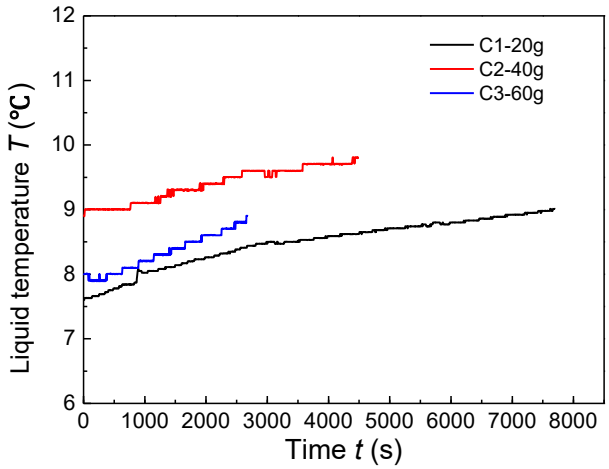

Fig. 8. The temperature of the fluid in the downstream water level control unit under different hyper-gravity levels (20 g, 40 g, and 60 g) for the single-fracture model.

0.9–1.4 °C, indicating that the influence of the temperature of the liquid on the hydrodynamic viscosity coefficient can be ignored.

3.2. Test 2: Fracture network model

3.2.1. The effect of hyper-gravity on the flow behavior

Fig. 9 shows the pore water pressure/water level in the effluent reservoir for the fracture network model under normal gravity and hyper-gravity. As shown in Fig. 9a, the pressure and water level in the N1, N2, and N3 experiments increase linearly, and the slope increases with an increase in the pressure difference, the same as for the single-fracture model. Fig. 9b shows that the slopes of the pore pressure and water level increase linearly, indicating the flow velocity in the model remains unchanged. This result shows that the internal fracture structure of the 3D printed fracture network model remains relatively stable under hyper-gravity.

As shown in Fig. 4b, the data obtained from the transport experiments conform to the fitting curve obtained from the flow experiments in the fracture network model, indicating the flow characteristics of the solute transport in the 3D printed fractured network models are the same under 1 g and 80 g.

The flow velocity and equivalent hydraulic fracture aperture under different experimental conditions are listed in Table 4. The equivalent hydraulic fracture aperture is similar in the normal gravity and hyper-gravity experiments. The difference in the flow velocity between N2 and D1 is 0.97%, demonstrating that the flow characteristics of the 3D printed fracture network model are the same under hyper-gravity and normal gravity.

3.2.2. The effect of hyper-gravity on the transport behavior

Fig. 10 shows the cumulative conductivity/concentration curves and BTCs of the normal gravity (N2) and hyper-gravity experiments (D1) for the fracture network model. As shown in Fig. 10a, the conductivity curves exhibit fluctuation under 80 g hyper-gravity. The sudden decrease at the end of the cumulative concentration curve may be due to the high centrifugal acceleration, which significantly affects the working performance of the conductivity sensor. In addition, the characteristics of the cumulative concentration curve are similar under 1 g and 80 g. The BTCs are slightly different, but the overall difference is small, indicating that the solute transport characteristics in the 3D printed fracture network model are similar under hyper-gravity and normal gravity.

The calculated breakthrough time $t_{0.1}$ and *Pe* for different experimental cases are given in Table 4. The breakthrough time of the solute decreases with an increase in the pressure in the normal gravity experiments.

The fitting results of the normalized BTCs for N2 and D1 are shown in Fig. 11, and the ADE fitting D_h and R^2 are listed in Table 4. The R^2 values are greater than 0.98, and the D_h increases with increasing pressure. The relative difference between N2 and D1 is 9.58%.

The temperature of the outflow liquid in the D1 experiment is shown in Fig. 12. The temperature increases over time. Although the centrifugal acceleration was high, the experimental duration was short. Thus, the maximum temperature difference was only 0.8 °C, indicating that the influence of the temperature on the hydrodynamic viscosity coefficient can be ignored.

In summary, based on the scaling law in previous study (Hensley and Schofield, 1991; Taylor, 1995; Levy et al., 2002, 2003; Jones et al., 2017), a small-scale hyper-gravity fracture model can achieve the gradient boundary condition of water pressure in a large-scale prototype, and then it is possible to reproduce the flow and transport process of the large-scale prototype. In this study, our results indicate that the hyper-gravity effect on the flow and solute transport characteristics of the 3D-printed single/fracture network models is small or non-existent for the range of G-levels tested, for accelerations of up to 80 g. This is to be expected because the flow and transport characteristics are related to the fracture model's properties (fracture aperture, fracture roughness, fracture geometry, etc.), and despite some variations in the structure of the fracture model due to compression during the centrifuge spinning, the Darcy's law represented by the permeability k and solute transport mechanism represented by D_f (diffusion coefficient) are not affected by

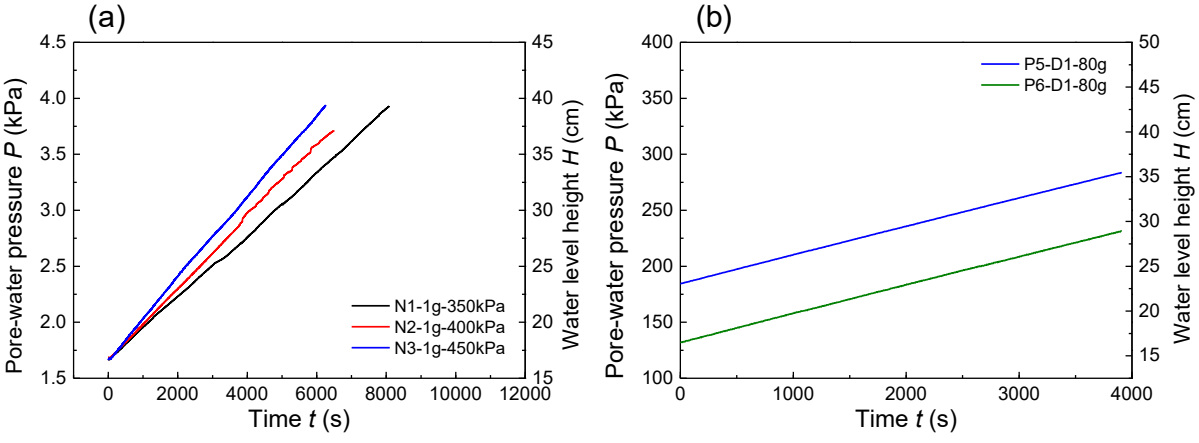

Fig. 9. Pore water pressure/water level in the downstream water level control unit for the fracture network model: (a) normal gravity; (b) hyper-gravity.

Table 4
Flow and solute transport characteristics in the 3D printed fracture network model under 1 g and 80 g.

G level	Case	v (10^{-1} m/s)	b_h (10^{-5}m)	Re	Pe	$t_{0.1}$ (s) ($C/C_0 = 10\%$)	D_h (10^{-5} m^2/s)	ADE fitting error R^2
1 g	N1	0.907	2.850	1.980	1273.801	895	1.38	0.9801
	N2	1.025	2.834	2.225	1431.658	641	1.67	0.9886
	N3	1.172	2.857	2.564	1649.747	449	1.79	0.9941
80 g	D1	1.016	2.801	1.179	1401.841	634	1.51	0.9872

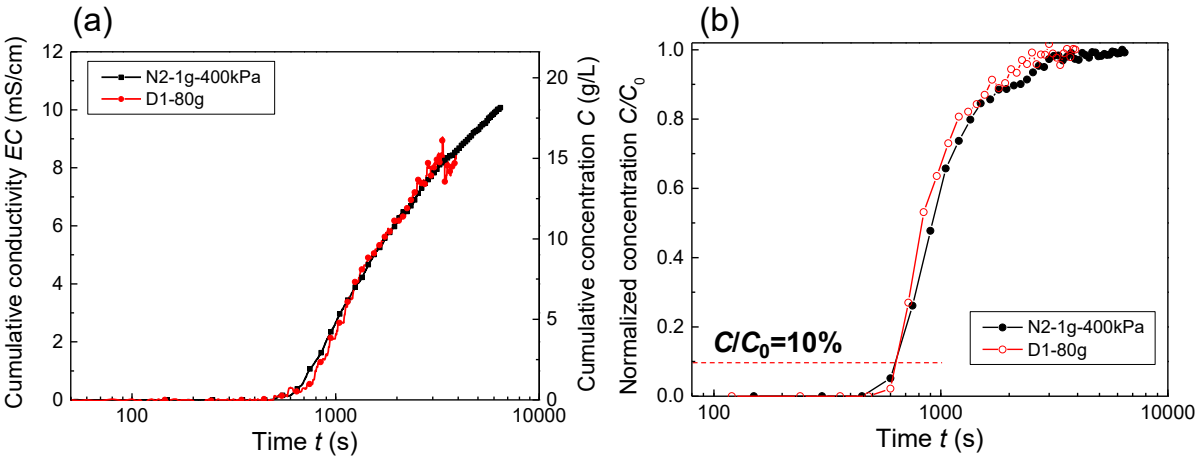

Fig. 10. Comparison of experimental results of normal gravity and hyper-gravity tests for the fracture network model: (a) cumulative conductivity/concentration curve; (b) outflow concentration curve.

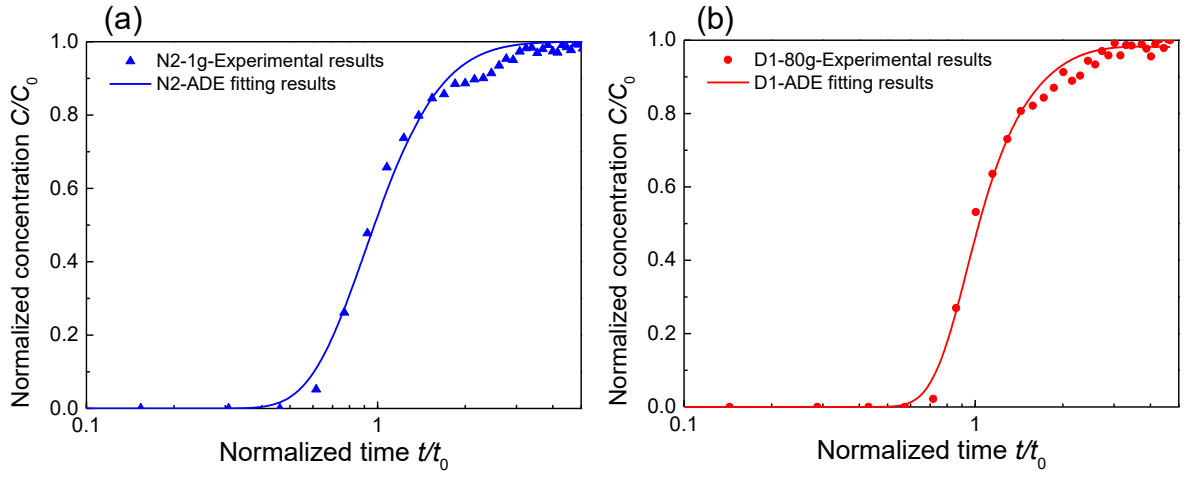

Fig. 11. Fitting curves of the normalized outflow concentration for the fracture network model: (a) normal gravity; (b) hyper-gravity (80 g).

gravity in a hyper-gravity environment. Furthermore, as to the authors knowledge, it is difficult to apply the gradient boundary condition of water pressure on the scaled model when conduct a 1 g scaled experiment. However, different to the 1 g scaled model experiment, the hyper-gravity experiment is an efficient method to reproduce the prototype gradient boundary condition, such as water pressure gradient, hydraulic boundary conditions. Therefore, the long-term migration of contaminants in the in-situ fractured rock mass can be simulated in a N g scaled model under hyper-gravity condition, and then the contaminant breakthrough curves at different outflow positions can be obtained to predict the contaminant breakthrough time. Thus, our results provide new insights into the experimental study of contaminant transport in a complex fracture model under hyper-gravity condition.

4. Evaluation method for long-term barrier performance

4.1. Method

Based on the results of the hyper-gravity experiments, we propose a long-term barrier performance evaluation method for low-permeability fractured rock masses, as shown in Fig. 13. The main steps are as follows.

Step 1: Determine the input parameters, including the geometric parameters (length, width, depth) of the research object, the hydrogeological conditions, the geometric parameters of the fracture (fracture trend, length, density, and size), the key solutes or contaminants, and the simulation parameters;

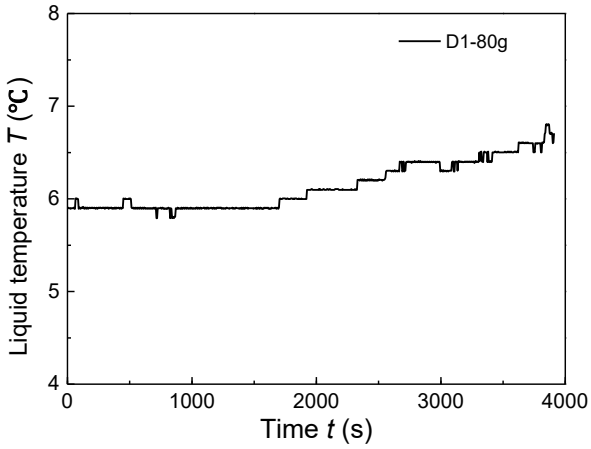

Fig. 12. The temperature of the liquid in the downstream water level control unit under 80 g for the fracture network model.

Step 2: Establish a simplified three-dimensional fracture network model according to the fractures' geometric parameters. Determine whether the influence of the rock matrix around the fracture and the sorption and decay processes should be considered;
Step 3: Carry out an OpenGeoSys (OGS) simulation to obtain the flow and concentration field, BTCs, and breakthrough time (T_t) or maximum breakthrough concentration (C_{max}). Assess whether the *Re* and Peclet number (*Pe*) meet the following conditions in the hyper-gravity experiments according to the previous study (Hensley and Schofield, 1991; Jones et al., 2017; Levy et al., 2002, 2003; Taylor, 1995): $Re \leq Re_{cr}$ (=1) and $Pe \leq Pe_{cr}$ (=1). If the conditions are met, proceed to Step 4; otherwise, optimize and adjust the fracture model or the boundary conditions, such as decrease the fracture aperture (or hydraulic permeability) of the model or decrease the hydraulic gradient between the inlet and outlet of the model;
Step 4: Create a 3D-printed fracture model and conduct a hyper-gravity experiment to evaluate the long-term barrier performance of the low-permeability fractured rock mass. Analyze the experimental results from the following two aspects: (1) If the contaminants are conservative solutes (such as chloride ions), the BTCs and breakthrough time (T_t) obtained from the experiments can be directly compared with the numerical simulation results to verify the long-term barrier performance of the low-permeability fractured rock mass. (2) If the contaminants are non-conservative solutes (such as heavy metal ions and nuclides), it is necessary to conduct additional theoretical analysis of the experimental results based on the sorption and decay parameters of the contaminants. Predict the prototype BTCs, breakthrough time (T_t) or maximum breakthrough concentration (C_{max}) to verify the long-term barrier performance of the low-permeability fractured rock mass.

4.2. Case study

We conducted a case study in Xinchang, Beishan, Gansu Province, using the proposed method to evaluate the 10,000-year transport of nuclides in high-level waste through the geological barrier. A simplified 3D fracture network model was generated based on the Monte Carlo simulation method. The solute transport process was simulated in the normal gravity 1 g prototype (Fig. 14a), the hyper-gravity 500 g scaled model (Fig. 14b), and the normal gravity 1 g scaled model (Fig. 14c) using the OGS software. The solute transport was compared under different conditions. The feasibility and required conditions for simulating the solute transport in a fractured rock mass with a hyper-gravity model were analyzed.

4.2.1. Numerical model and physical parameters

Fig. 15 shows the simplified randomly generated 3D fracture network model and corresponding mesh. The generation method has been described in detail by Hu et al. (2021). The model is 500 m long × 500 m wide × 500 m high.

Since it is difficult to simulate the pore structure characteristics of the rock matrix around fractures using 3D printing, such as the porosity and the decay of the nuclide, we only considered advection and dispersion in the fracture network in the hyper-gravity experiment. The influences of

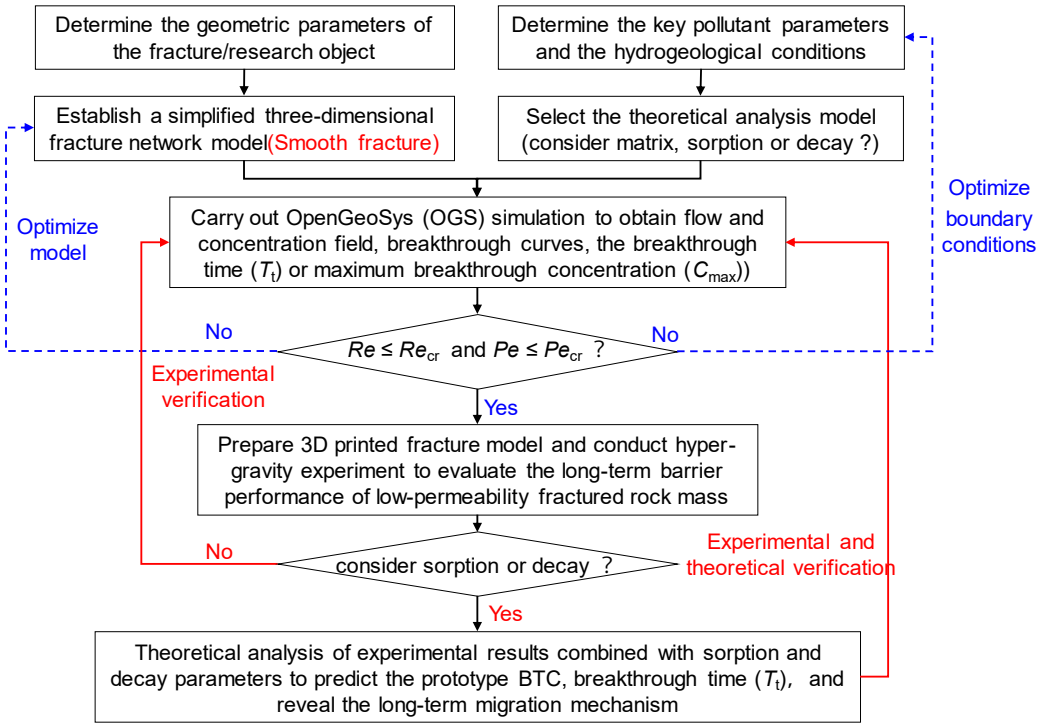

Fig. 13. Flowchart of the evaluation method for the long-term barrier performance of fractured rock masses based on a hyper-gravity experiment.

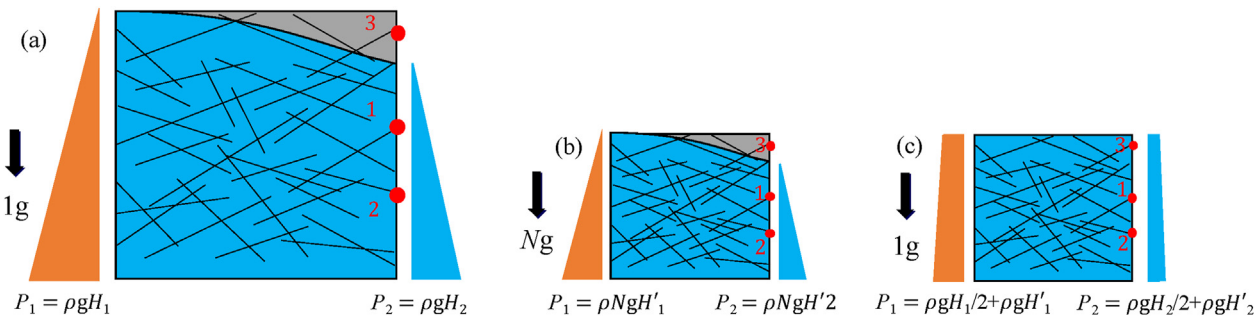

Fig. 14. Conceptual models of the fracture network model and boundary conditions for three numerical cases: (a) 1 g prototype; (b) 500 g scaled model; (c) 1 g scaled model.

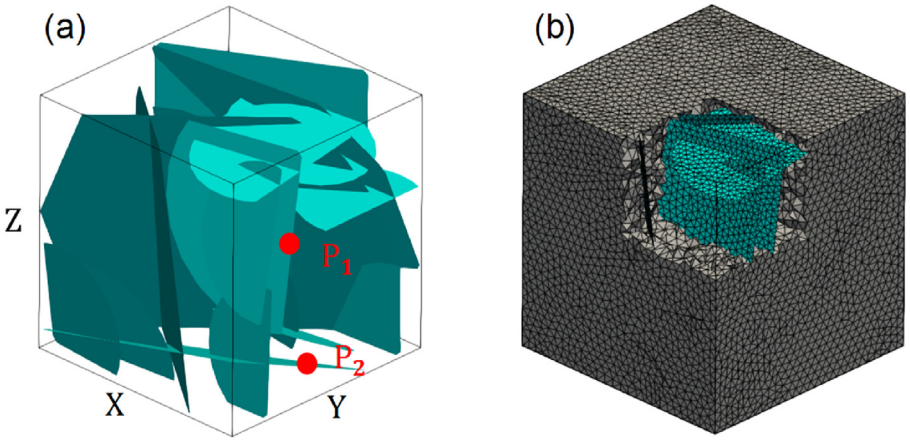

Fig. 15. Simplified 3D fracture network model and meshes.

sorption, decay, and other factors were predicted by analyzing the results.

Table 5 summarizes the simulated cases. Only advection and dispersion were considered in the fracture network of the 1 g prototype, 500 g scaled model, and 1 g scaled model. However, different physical and chemical processes were considered in the 1 g prototype to compare the influences of the factors on the solute transport process and determine the long-term performance of the geological barrier. In all cases listed in the table, the pollution sources with a concentration of 1 mol/L are continuously injected from the left boundary surface. In addition, the parameters of the pollution sources, such as the sorption allocation coefficient and decay coefficient, were selected from JNC-H12 (2000).

4.2.2. Case study results

We use the outflow position $P_{1,\ p}$ (500 m, 139 m, 409 m) as an example. The BTCs considering the matrix diffusion, sorption, decay, and other physical and chemical processes in the 1 g prototype are shown in Fig. 16. In general, the BTCs exhibit a shift to the right when the matrix diffusion, adsorption, and decay are considered. At a concentration of $C/C_0 = 10\%$, the breakthrough time is 39.7 years when only advection and dispersion are considered. When advection and dispersion of the fracture network and the surrounding matrix are considered, the breakthrough time is 41,200 years because the molecular diffusion in the matrix significantly extends the breakthrough time of the contaminants. The breakthrough time is 729,300 years when advection, diffusion, and sorption are considered. The breakthrough time of the contaminants is prolonged by the interface between the fracture and matrix and the sorption of contaminants by the matrix. When advection, diffusion, adsorption, and decay are considered, the breakthrough time of the model does not change much, but the maximum breakthrough

Table 5
Numerical simulation settings.

Case	1 g prototype	500 g scaled model	1 g scaled model
A: advection + dispersion (no matrix)	✓	✓	✓
B: advection + dispersion (with matrix)	✓	–	–
C: advection + dispersion + sorption (with matrix)	✓	–	–
D: advection + dispersion + sorption + decay (with matrix)	✓	–	–

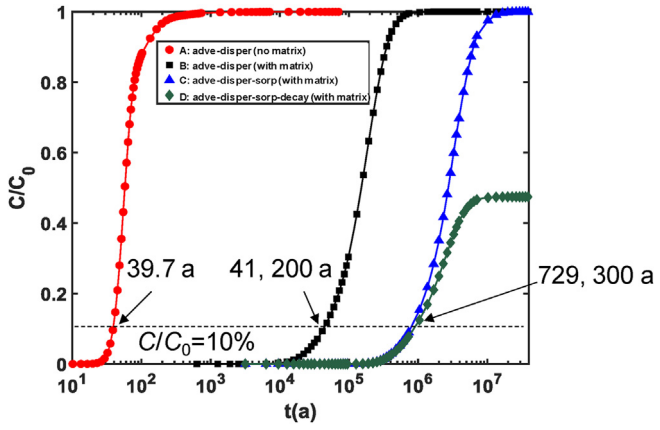

Fig. 16. Comparison of the BTCs at outlet P_1 with different physicochemical processes.

concentration of the contaminants is reduced by 47% due to decay. Therefore, it is feasible to evaluate the long-term barrier properties of the fractured rock mass with low permeability by considering only the advection and diffusion effect in the fracture network, i.e., the prototype. The scaled model can be used for hyper-gravity experiments for comparison and verification, and the matrix effect, sorption, and decay can be evaluated by numerical simulation. We assessed the numerical simulation results of the 1 g prototype, 500 g scaled model, and 1 g scaled model to determine the feasibility of the hyper-gravity experiment.

Fig. 17 shows the pressure, velocity, and concentration fields derived from the model at 80 years of the prototype. The pressure and concentration fields of the 1 g prototype and 500 g scaled model are the same, and the velocity field is similar (model: prototype = 500:1). However, the simulation results of the 1 g prototype and 1 g scaled model are significantly different.

We created the BTCs for the outflow positions of the prototype model $P_{1,\ p}$ (500 m, 139 m, 409 m), $P_{2,\ p}$ (500 m, 157 m, 110 m), the scaled model $P_{1,\ m}$ (1 m, 0.278 m, 0.818 m), and $P_{2,\ m}$ (1 m, 0.314 m, 0.220 m) to quantify to solute concentrations for different cases. The results of the 1 g scaled model and 500 g scaled model were scaled according to the N^2 (model: prototype) time similarity ratio, as shown in Fig. 18. It is observed that the trends of the BTCs of the 1 g prototype and the 500 g scaled model are identical. However, the trend of the BTC of the 1 g scaled model differs substantially from that of the 1 g prototype. The reason is that the flow field was different in the 1 g scaled model, resulting in different concentrations. The results show that it is difficult to simulate the flow and solute transport processes in the 1 g prototype with the 1 g scaled model.

Table 6 lists the average flow velocity, *Re*, and *Pe* values for different cases. The *Re* for the three cases were smaller than $Re_{cr} = 1$, conforming to the assumption of flow similarity. The average velocity ratio between the 500 g scaled model and the 1 g prototype was 501.3:1, similar to the theoretical flow rate (model: prototype = 500: 1). The *Pe* of the 500 g scaled model was also smaller than $Pe_{cr} = 1$. These findings, combined with the concentration field and the BTCs, show that the mechanical dispersion was similar for the 500 g scaled model and the 1 g prototype.

Based on these results and the similarity of the fracture aperture, the feasibility and required conditions of the hyper-gravity experiments of solute transport in a fractured rock mass are summarized in Table 7. In the smooth fracture model, the advection process is characterized by laminar flow, and the hydrodynamic dispersion is dominated by molecular diffusion when the similarity ratio of the fracture aperture between the prototype and the model is 1:1 (the similarity ratio of the permeability coefficient is 1:1), and the *Re* and *Pe* are less than the critical value. The mechanical dispersion can be ignored; thus, the 500 g scaled experiments can reproduce the flow and solute transport processes of the 1 g prototype. Therefore, if the flow and solute transport processes are similar, the long-term barrier performance of the fractured rock mass with low permeability can be verified by hyper-gravity experiments to reveal the long-term solute transport through the geological barrier to improve the theoretical model.

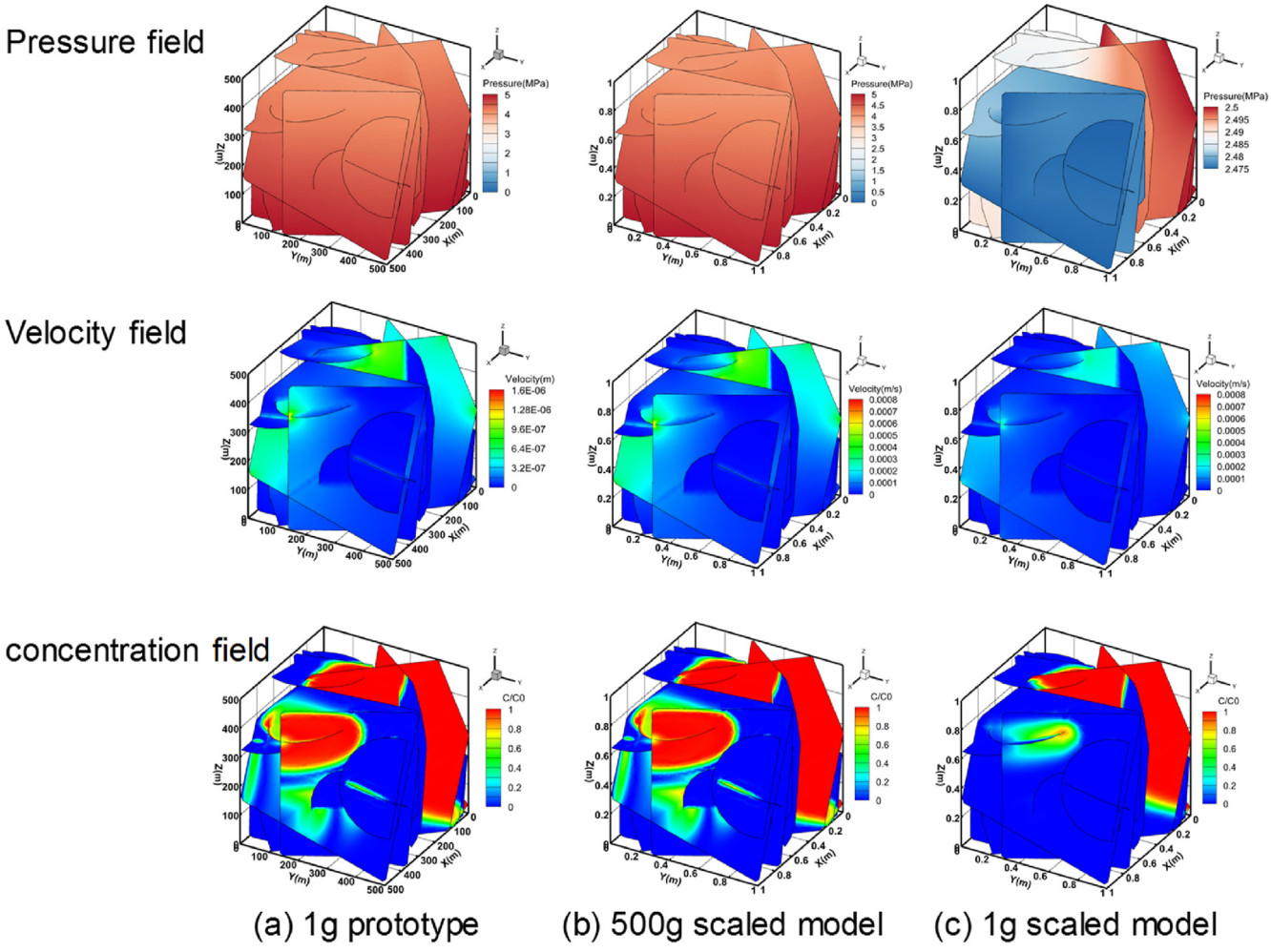

Fig. 17. Comparison of pressure, velocity, and concentration field for the 1 g prototype, 500 g scaled model, and 1 g scaled model (the model time is converted to the prototype scale).

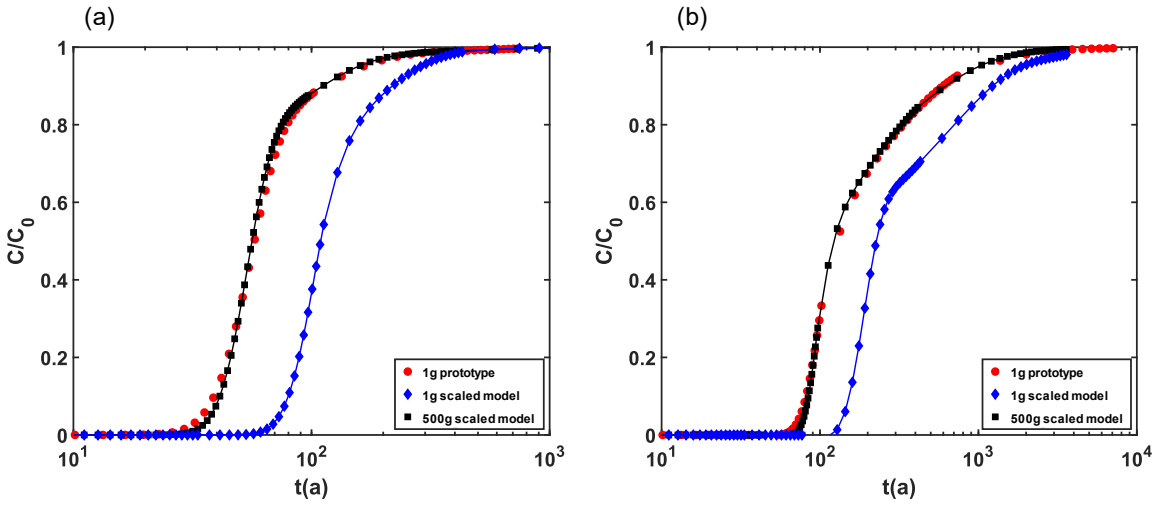

Fig. 18. Comparison of the outflow concentration of the 1 g prototype, 1 g scaled model, and 500 g scaled model: (a) outlet P_1; (b) outlet P_2.

Table 6
Calculation results of numerical simulation.

Case	1 g prototype	500 g scaled model	1 g scaled model
Flow rate (m/s)	1.66×10^{-7}	8.32×10^{-5}	4.26×10^{-5}
Reynolds number (*Re*)	1.58×10^{-6}	7.92×10^{-4}	4.06×10^{-4}
Peclet number (*Pe*)	0.00082	0.41	0.21

Table 7
Feasibility and conditions for the hyper-gravity experiment of solute transport in a fractured rock mass.

Process	Conditions	Similarity ratio of physical parameters	Similarity ratio of the time scale	Feasibility
Advection	Laminar flow ($Re \leq Re_{cr}$)	$K = 1$ ($b = 1$)	$t = 1/N^2$	✓
Mechanical dispersion	Diffusion dominated ($Pe \leq Pe_{cr}$)	$D_m = N$	$t = 1/N^3$	✓
Molecular diffusion	–	$D_d = 1$	$t = 1/N^2$	✓
Sorption	Instantaneous equilibrium adsorption	$K_f = 1$	$t = 1/N^2$	✓

Notes: K_f represents the sorption partition coefficient.

5. Conclusions

Normal gravity and hyper-gravity experiments of the solute transport in fractured rock were conducted with a sealed control apparatus containing 3D-printed single/fractured network models. The flow and solute transport characteristics of the fracture model were obtained under different pressures and g levels. The flow velocity, cumulative concentration curves, and BTCs under normal gravity and hyper-gravity were compared, and the fitting results of the BTCs were discussed. Subsequently, a new method for evaluating the long-term barrier performance of a low-permeability fractured rock mass using a hyper-gravity experiment was proposed. The feasibility of this method to simulate nuclide transport in a deep geological disposal reservoir was discussed. The following conclusions were obtained.

(1) The pore water pressure and water level increased linearly over time, indicating that the flow velocity in the model was unchanged. The difference in the flow velocity between the normal gravity and hyper-gravity experiments ranged from 0.97 to 3.12%, suggesting that the internal fractures of the 3D printed single/network fracture models under hyper-gravity were relatively stable, and the flow characteristics remained the same. The trends of the cumulative concentration were consistent in the normal gravity and hyper-gravity experiments, and the BTCs were slightly different. The difference in the fitted hydrodynamic dispersion coefficient between the experiments ranged from 9.09 to 20.4%, demonstrating that the solute transport characteristics in the 3D printed single/network fracture models under hyper-gravity were within the acceptable range.

(2) The results of the normal gravity and hyper-gravity experiments showed that the solute transport in the fractured rock mass was affected by the fracture aperture, roughness, and geometry but not by hyper-gravity. Therefore, hyper-gravity experiments can be used to simulate the water pressure gradient, hydraulic boundary conditions, and solute transport in fractured rock masses.

(3) OGS software was used to simulate and analyze the flow and solute transport in the 1 g prototype, the 1 g scaled model, and the 500 g scaled model. The BTCs of the fracture network model were compared at different outflow locations and simulation conditions. The results showed that the hyper-gravity experiment could reproduce the flow and solute transport in the normal gravity prototype when $Re \leq Re_{cr}$ and $Pe \leq Pe_{cr}$. Our results provide technical support for studying the solute transport characteristics in large-scale complex fracture network models and predicting the breakthrough of contaminants such as nuclides in fractured rock masses. The proposed method is suitable for verifying the long-term barrier performance of deep earth projects, such as deep geological disposal.

In this study, to systematically investigate the hyper-gravity effect on fluid flow and solute transport in fractured rock, we only consider the parallel fracture model. However, in real conditions, rough-walled fracture is more frequently (Zhan et al., 2022a,b; Zou and Cvetkovic, 2020; Dou et al., 2019; Huang et al., 2019; Ye et al., 2017; Makedonska et al., 2016). Therefore, more realistic conditions with the consideration of fracture roughness in rough-walled fracture is needed for further studies in the future. More importantly, the hyper-gravity similarity in the rough-walled fracture is still an open question, before applying the geotechnical centrifuge modelling technique to replicate the flow and transport processes in real fractured rocks, continued research about the similarity of flow and transport in complex fractured rocks is necessary. In addition, further research is also required for higher G-levels of

centrifuge gravity or different flow regimes such as non-Darcy's flow.

Declaration of competing interest

The authors declare that they have no known competing financial interests or personal relationships that could have appeared to influence the work reported in this paper.

Acknowledgements

The study is financially supported by the Basic Science Center Program for Multiphase Evolution in Hypergravity of the National Natural Science Foundation of China (No. 51988101), the National Key Research and Development Project China (No. 2018YFC1802300), the National Natural Science Foundation of China (No. 42007262) and the National Natural Science Foundation of China (No. 42277128).

References

Arulanandan, K., et al., 1988. Centrifuge modeling of transport processes for pollutants in soils. Journal of Geotechnical Engineering-ASCE 114 (2), 185–205.
Brouwers, L.B., Dippenaar, M.A., 2018. Partially Saturated Flow from Sand into a Discrete Smooth Open Vertical Fracture at the Soil–Rock Interface: Experimental Studies. Bulletin of Engineering Geology and the Environment.
Chen, Y., Han, C., Ling, D., Kong, L., Zhou, Y., 2011. Development of geotechnical centrifuge ZJU400 and performance assessment of its shaking table system. Chin. J. Geotech. Eng. 33 (12), 1887–1894.
Costin, L.S., 1997. Site Selection and Characterization Processes for Deep Geologic Disposal of High Level Nuclear Waste. office of scientific & (technical information technical reports).
Dou, Z., Sleep, B., Zhan, H., Zhou, Z., Wang, J., 2019. Multiscale roughness influence on conservative solute transport in self-affine fractures. Int. J. Heat Mass Tran. 133, 606–618.
Griffioen, J.W., Barry, D.A., 1999. Centrifuge modeling of unstable infiltration and solute transport. J. Geotech. Geoenviron. Eng. 125 (7), 556–565.
Gurumoorthy, C., Singh, D.N., 2004. Centrifuge Modeling of diffusion through rock mass. J. Test. Eval. 33 (1), 44–50.
Hensley, P.J., Schofield, A.N., 1991. Accelerated physical modelling of hazardous-waste transport. Geotechnique 41 (3), 447–466.
Huang, N., Jiang, Y., Liu, R., Li, B., Sugimoto, S., 2019. A novel three-dimensional discrete fracture network model for investigating the role of aperture heterogeneity on fluid flow through fractured rock masses. Int. J. Rock Mech. Min. Sci. 116, 25–37.
Jones, B.R., Brouwers, L.B., Tonder, W.D.V., Dippenaar, M.A., 2017. Assessing geotechnical centrifuge modelling in addressing variably saturated flow in soil and fractured rock. Environ. Sci. Pollut. Res. Int. 24 (15), 1–21.
Jones, B.R., Van Rooy, J.L., Dippenaar, M.A., 2018. Lugeon Tests at Partial Saturation: Experimental and Empirical Contributions. Rock Mechanics and Rock Engineering.
Kumar, R.P., Singh, D.N., 2012. Geotechnical centrifuge modeling of chloride diffusion through soils. Int. J. GeoMech. 12 (3), 327–332.
Laverov, N.P., Omelianenko, B.L., Velichkin, V.I., 1994. Geological Aspects of the Nuclear Waste Disposal Problem. office of scientific & technical information technical reports.
Levy, L., Culligan, P., Germaine, J., 2003. Modelling of DNAPL behavior in vertical fractures. International Journal of Physical Modelling 3 (1), 1–19.
Levy, L.C., Culligan, P.J., Germaine, J.T., 2002. Use of the geotechnical centrifuge as a tool to model dense nonaqueous phase liquid migration in fractures. Water Resour. Res. 38 (8), 34-1-34-12.
Lo, I.M.C., Hu, L.M., Meegoda, J.N., 2004. Centrifuge modeling of light nonaqueous phase liquids transport in unsaturated soils. J. Geotech. Geoenviron. Eng. 130 (5), 535–539.
Makedonska, N., et al., 2016. Evaluating the effect of internal aperture variability on transport in kilometer scale discrete fracture networks. Adv. Water Resour. 94, 486–497.
Mckinley, I.G., Alexander, W.R., Blaser, P.C., 2007. Development of geological disposal concepts. Radioact. Environ. 9 (6), 41–76.
Ng, C.W.W., 2014. The state-of-the-art centrifuge modelling of geotechnical problems at HKUST. Journal of Zhejiang University. A. Science 15 (1), 1–21.
Nishimoto, S., Sawada, M., Okada, T., 2016. New rapid evaluation for long-term behavior in deep geological repository by geotechnical centrifuge. Part 1: test of physical modeling in near field under isotropic stress-constraint conditions. Rock Mech. Rock Eng. 49 (8), 3323–3341.
Sawada, M., Nishimoto, S., Okada, T., 2017. New rapid evaluation for long-term behavior in deep geological repository by geotechnical centrifuge—Part 2: numerical simulation of model tests in isothermal condition. Rock Mech. Rock Eng. 50 (1), 159–169.
Schofield, A.N., 1980. Cambridge geotechnical centrifuge operations. Geotechnique 30 (3), 227–268.
Soga, K., Kawabata, J., Kechavarzi, C., Coumoulos, H., Waduge, W.A.P., 2003. Centrifuge modeling of nonaqueous phase liquid movement and entrapment in unsaturated layered soils. J. Geotech. Geoenviron. Eng. 129 (2), 173–182.
Taylor, R.N., 1995. Geotechnical Centrifuge Technology. CRC Press.
Wang, J., Chen, L., Su, R., Zhao, X., 2018. The Beishan underground research laboratory for geological disposal of high-level radioactive waste in China: planning, site selection, site characterization and in situ tests. J. Rock Mech. Geotech. Eng. 10 (3), 411–435.
Ye, Z., Liu, H., Jiang, Q., Liu, Y., Cheng, A., 2017. Two-phase flow properties in aperture-based fractures under normal deformation conditions: analytical approach and numerical simulation. J. Hydrol. 545, 72–87.
Zhan, L., et al., 2022a. Effects of multiscale heterogeneity on transport in three-dimensional fractured porous rock with a rough-walled fracture network. Comput. Geotech. 148, 104836.
Zhan, L., You, Y., Zhao, R., Chen, C., Chen, Y., 2022b. Centrifuge modelling of retardation of Pb^{2+} migration in loess–amended soil–bentonite barriers. Int. J. Phys. Model. Geotech. 1–35.
Zou, L., Cvetkovic, V., 2020. Inference of transmissivity in crystalline rock using flow logs under steady-state pumping: impact of multiscale heterogeneity. Water Resour. Res. 56 (8).